

Geophysical Research Letters*

-

RESEARCH LETTER

10.1029/2025GL114717

Special Collection:

Holocene climate changes: process, mechanism and impacts

Key Points:

- New cave records from Russian Far East show a synchronous δ¹⁸O negative excursion and intensified monsoon precipitation between 8 and 9 ka BP
- The change in rainfall and speleothem δ¹⁸O in Northeast Asia contrasts with patterns observed in North China during early to mid-Holocene
- The findings suggest that Northern Hemisphere summer insolation played a primary role in shaping this contrasting pattern

Supporting Information:

Supporting Information may be found in the online version of this article.

Correspondence to:

H. Cheng and S. A. Gorbarenko, cheng021@mail.xjtu.edu.cn; gorbarenko@poi.dvo.ru

Citation:

Wang, K., Zhao, J., Cai, Y., Zhang, H., Li, H., Zhang, X., et al. (2025). Contrasting responses of monsoon rainfall and speleothem oxygen isotope between Northeast Asia and North China during the early-mid Holocene. *Geophysical Research Letters*, 52, e2025GL114717. https://doi.org/10.1029/2025GL114717

Received 27 JAN 2025 Accepted 30 SEP 2025

© 2025. The Author(s). This is an open access article under the terms of the Creative Commons Attribution License, which permits use, distribution and reproduction in any medium, provided the original work is properly cited.

Contrasting Responses of Monsoon Rainfall and Speleothem Oxygen Isotope Between Northeast Asia and North China During the Early-Mid Holocene

Kexin Wang¹, Jingyao Zhao¹, Yanjun Cai¹, Haiwei Zhang¹, Hanying Li¹, Xu Zhang², Xiaojian Zhang³, Jian Wang¹, Sergey A. Gorbarenko⁴, Yuriy I. Bersenev⁵, Yuriy P. Vasilenko⁴, and Hai Cheng¹

¹Institute of Global Environmental Change, Xi'an Jiaotong University, Xi'an, China, ²Ice Dynamics and Paleoclimate, British Antarctic Survey, Cambridge, UK, ³School of Geography and Ocean Science, Nanjing University, Nanjing, China, ⁴V.I. Il'ichev Pacific Oceanological Institute, Far Eastern Branch of the Russian Academy of Science, Vladivostok, Russia, ⁵Primorsky Branch of the Russian Geographical Society, Vladivostok, Russia

Abstract A critical gap in East Asian summer monsoon research is the lack of speleothem records from its northeasternmost fringe, hindering tests of orbital-scale monsoon variability at higher latitudes. Our new records from the Russian Far East, spanning 9–5 ka BP, fill this spatial gap and reveal a synchronous $\delta^{18}O$ negative excursion and intensified monsoon precipitation between 8 and 9 ka BP, contrasting with trends in North China. We suggest this difference may stem from changes in Northern Hemisphere summer insolation (NHSI) over the Holocene. The NHSI decrease since early Holocene weakens southwesterly winds and the Western Pacific Subtropical High, shifting the westerly jet and rainbelt southward. This causes reduced (increased) precipitation in North China (Northeast Asia), as well as reduced (increased) contribution of Pacific Ocean moisture to North China (Northeast Asia), resulting in $\delta^{18}O$ increase (decrease) in North China (Northeast Asia).

Plain Language Summary Speleothem oxygen isotope (δ^{18} O) records are widely used as high-resolution proxies to characterize East Asian summer monsoon (EASM) variability at various timescales. While discrepancies between coherent δ^{18} O records and regionally inconsistent moisture patterns have been identified, studies on the eastern edge of the EASM region remain sparse. This study provides new cave records from the Russian Far East, covering 9 to 5 ka BP, the northernmost site in the EASM region. Combined with other records from Northeast Asia, we observe significant synchronous depletion of speleothem δ^{18} O and intensified monsoon precipitation in Northeast Asia between 8 and 9 ka BP. This contrasts with patterns in North China. We suggest that this contrast is driven by changes in the Northern Hemisphere Summer Insolation (NHSI) during the Holocene. A decrease in NHSI weakens the southwesterly winds and the West Pacific Subtropical High, while simultaneously inducing a southward shift of the westerly jet. These changes collectively force the East Asian rain belt southward. This leads to reduced precipitation in North China and increased rainfall in Northeast Asia, along with δ^{18} O enrichment in North China and depletion in Northeast Asia. These findings offer a more spatially detailed understanding of the EASM region's footprint from North China to Northeast Asia during the Holocene.

1. Introduction

The East Asian summer monsoon (EASM) is a critical component of the global climate system, profoundly influencing the ecological and environmental conditions across East Asia. The high-resolution and precisely dated speleothem records have greatly advanced our understanding of the climate variability of the Asian summer monsoon (ASM) from orbital to decadal timescales, as well as their global teleconnections (Y. Cai et al., 2015; Cheng et al., 2006, 2009, 2016; Y. Wang et al., 2001, 2005, 2008; Yuan et al., 2004). However, a closer examination of speleothem records reveals that the majority of the data are concentrated in the core region of the EASM, where these records exhibit the coherent variability on orbital timescales. Yet, recent studies indicate exceptions to this spatial consistent pattern. For instance, H. Zhang et al. (2021) highlighted that the speleothem δ^{18} O record in Shennong Cave in southeastern China has remained stable over the entire Holocene, thus suggesting a spatiotemporal diversity in speleothem δ^{18} O across monsoonal China, which is related to the latitudes shifts of convective precipitation in the monsoon frontal system. Furthermore, from a modern climate perspective,

WANG ET AL. 1 of 13

the EASM is not confined to East China but extends beyond, encompassing the Meiyu-Baiu rainband that spans East China, the Korean Peninsula, and Japan, thereby covering a much larger region. A recent study (Q. Wen et al., 2024) highlighted a grand dipole pattern of oxygen isotope and rainfall between South Asia and Japan region, with South China lying in a hybrid transition region on orbital-scales. It further suggested that the mismatch between rainfall and oxygen isotopes is an inherent characteristic of the ASM variability. However, this perspective lacks direct supporting evidence, since speleothem δ^{18} O data on orbital-scales from Northeast Asia, including Northeast China, Japan and the Korean Peninsula, remain sparse or limited in duration.

On the other hand, the Holocene records from loess deposits (Lu et al., 2013; H. Wang et al., 2014), dune percentages (Lu et al., 2005; Xu et al., 2020), paleosol development (Q. Li et al., 2014), and vegetation reconstructions (Chen et al., 2015; R. Wen et al., 2017) suggest that the EASM precipitation maximum was between ~5 and 2.4 ka on the western Chinese Loess Plateau, while it peaked around ~6 ka in northern China. They suggest that the EASM intensity (in terms of rainfall) was likely delayed and/or modulated by internal feedback processes, such as the effects of change in high-northern-latitude ice sheets, atmospheric CO_2 (Lu et al., 2013), and Atlantic Meridional Overturning Circulation (AMOC) (Chen et al., 2015). Notably, the synchronous speleothem $\delta^{18}O$ records that closely mirror Northern Hemisphere Summer Insolation (NHSI) without significant phase lag, revealed that the EASM (in terms of dynamic) was dominantly driven by precession-induced insolation variations at orbital-scales (Cheng et al., 2016; Y. Wang et al., 2005). This discrepancy may come from the complexity of $\delta^{18}O$ as a hydroclimate proxy, as it integrates dynamic monsoon processes (e.g., upstream rainout, vapor-source shifts) rather than solely reflecting local precipitation amount (Cheng et al., 2019; H. Zhang et al., 2021). Therefore, the discrete and dynamic nature of the monsoon calls for a systematic understanding of how the different components of the monsoon system interact and the driving mechanisms behind its variability via a view of the "monsoon system science" (Cheng et al., 2021, 2022).

In this study, we have successfully collected two speleothems from northeastern Vladivostok in the southern Russian Far East, providing the northernmost (the highest latitude hitherto) speleothem record from the EASM domain with Pacific moisture contributions dominate. By integrating these records with existing data, we aim to investigate the climate variability in the Northeast Asia region from the early- to mid-Holocene, and to investigate latitudinal gradients in EASM responses to orbital-scale forcing—a critical yet understudied dimension in current speleothem-based paleomonsoon reconstructions.

2. Cave and Modern Climatology

Two speleothems were collected from Sadovaya Cave ($44^{\circ}27'38''N$, $135^{\circ}42'01''E$, 450 m above sea level) and Tetukhe Cave ($44^{\circ}36'40''N$, $135^{\circ}32'00''E$, 390 m above sea level), and both, approximately 23 km apart, are located in 335 km northeast of Vladivostok City, in the southern part of the Sikhote-Alin of the Russian Far East (Figure 1). The caves are formed in Triassic limestones with similar geological characteristics. Sadovaya Cave has a narrow entrance measuring 1 m in width and 1.2 m in height. The cave roof is approximately 10-12 m thick. This cave presents rather closed relict formation and a stable microclimate with consistently positive temperatures maintains throughout the year, ranging from +4 to $+5^{\circ}$ C. Humidity levels remain high year-round, between 96% and 100%. Tetukhe Cave, in contrast, has a larger entrance that transits into a narrow passage. The roof thickness at the sampling site exceeds 20 m. With a total length of over 1 km, it is a lengthy and narrow cave system formed along fault lines. This cave is relatively open, leading to a measurable temperature fluctuation. During summer, the temperatures range from +3 to $+4^{\circ}$ C, while in winter, they drop to approximately $-2-0^{\circ}$ C. The humidity levels approach 100% in summer but decrease to 80%-90% in winter.

The climate of the southern Russian Far East is strongly influenced by the East Asian monsoon system (Belyanin & Belyanina, 2021). The study site experiences a mean annual temperature of 4° C and annual precipitation of 697 mm during 1980–2020, based on isoGSM2 simulations (Yoshimura et al., 2008) (Figure 1d, the detailed information of ISOGSM2 can be found in Text S1 in Supporting Information S1). Approximately 50% of the annual rainfall occurs during the summer monsoon season (June–September, JJAS), while winter season contributes ~19%. Precipitation δ^{18} O values exhibit pronounced seasonal variations, with the lowest values in winter (<-14%) and the highest in summer (-8% to -10%).

The humid climate supports extensive boreal (taiga) and temperate (cool mixed) forests, which collectively cover over half of the area (Mokhova et al., 2009). Vegetation is predominantly composed of spruce and fir-spruce taiga forests, while cool mixed broadleaf-conifer forests are prevalent in the southern areas at elevations of 800–900 m.

WANG ET AL. 2 of 13

1944807, 2025, 20, Downloaded from https://agupubs.onlinelibrary.wiley.com/doi/10.1029/2025GL1.14717 by British Antarctic Survey, Wiley Online Library on [16/10/2025]. See the Terms and Conditions (https://onlinelibrary.wiley.com/terms-and-conditions) on Wiley Online Library for rules of use; OA

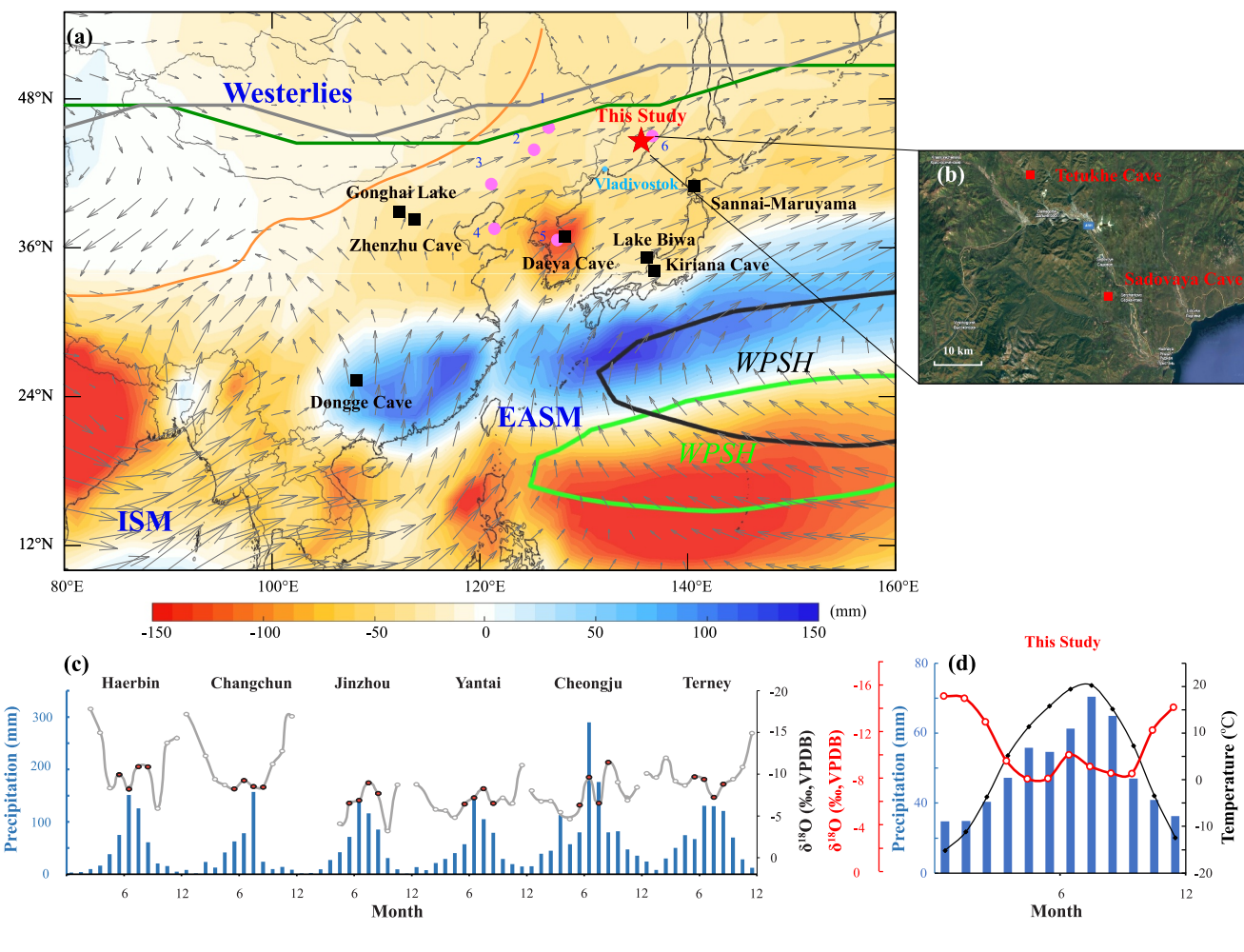


Figure 1. Locations of Tetukhe Cave, Sadovaya Cave, and other sites mentioned in the text, along with relevant regional climate information. (a) Atmospheric circulation and precipitation seasonality: Gray arrows depict the mean 850 hPa summer (June-July-August, JJA) streamline patterns based on NCEP/NCAR Reanalysis data (1980–2020). Shaded areas represent differences in precipitation (mm) between May-June and July-August based on GPCC data (1980–2020). The green and black contours show the average position of the West Pacific Subtropical High (WPSH) for May-June and July-August, respectively, represented by 5,880 geopotential meters (gpm) at 500 hPa, based on NCEP/NCAR Reanalysis data (1980–2020). The dark green and gray lines depict the climatological axis of the westerly jet at 200 hPa for May-June and July-August, respectively, defined by the line of maximum zonal wind speed (u-max) based on NCEP/NCAR Reanalysis data (1980–2020). The red star marks the study region (Russian Far East, encompassing Tetukhe and Sadovaya Caves). "EASM," "ISM," and "Westerlies" indicate areas primarily influenced by the East Asian Summer Monsoon, Indian Summer Monsoon, and Westerlies, respectively. The modern Asian summer monsoon boundary is shown as an orange line. Black squares denote key sites discussed in the text, and pink dots represent GNIP (Global Network of Isotopes in Precipitation) stations: 1. Haerbin; 2. Changchun; 3. Jinzhou; 4. Yantai; 5. Cheongju; 6. Terney. (b) Map showing the locations of Tetukhe Cave and Sadovaya Cave. (c) Modern precipitation δ¹⁸O and precipitation values from GNIP stations: Precipitation δ¹⁸O values (‰, V-PDB) and total precipitation amounts (mm) from the GNIP stations labeled in (a) (data source: https://www.iaea.org/services/networks/gnip). (d) Precipitation δ¹⁸O (‰, V-PDB), temperature (°C), and precipitation amounts (mm) from outputs of the isoGSM2 isotope-enabled atmospheric general circulation model (Yoshimura et al., 2008), used in this study to contextualize modern precipitatio

3. Materials, Age Model and Results

3.1. Speleothem Sample

Speleothem Sadovaya-S1 (~12.8 cm long), was sampled 74 m from Sadovaya Cave entrance, while speleothem Tetukhe-T1 (12.6 cm long), was sampled 54 m from Tetukhe Cave entrance. Both samples are pure calcite, cut along the growth axis, and polished. ^{230}Th dating, $\delta^{13}\text{C}$, and $\delta^{18}\text{O}$ analyses were performed on both.

3.2. Chronology

The results show that Tetukhe-T1 grew continuously between 7.80 ± 1.04 and 6.00 ± 0.80 ka BP (Figure S1a in Supporting Information S1). The samples are impure, with 230 Th/ 232 Th ratios ranging from 0.000028 to

WANG ET AL. 3 of 13

0.000058. Sadovaya-S1 grew continuously between 8.80 ± 0.05 and 7.43 ± 0.06 ka BP (Figure S1c in Supporting Information S1). The sample are also impure, with 230 Th/ 232 Th ratios ranging from 0.0002 to 0.001. The StalAge Monte-Carlo model (Scholz & Hoffmann, 2011) was used to establish the age models for the two samples (Figure S1 in Supporting Information S1).

3.3. Stable Isotopes of Oxygen and Carbon

The δ^{13} C and δ^{18} O values along the growth layers of both Tetukhe-T1 and Sadovaya-S1 (Figure S2 in Supporting Information S1) remain virtually constant, indicating that isotopic fractionation conditions (equilibrium or disequilibrium) were relatively stable during deposition, and drip water δ^{18} O may have been consistent over this period (Hendy test, Hendy & Wilson, 1968). For Tetukhe-T1, δ^{18} O values rang from -8.5% to -10.5%, with no significant long-term trend observed between 5.71 and 8.49 ka BP (Figure S3 in Supporting Information S1). The δ^{13} C values fluctuate between -6.2% and -8.1%. For Sadovaya-S1, the δ^{18} O values exhibit a negative shift of 0.8%, with an average of -5.94% from 9.0 ka BP to 8.6 ka BP, decreasing to -6.75% after approximately 8.6 ka BP. Similarly, δ^{13} C values show a negative shift of 2.2%, averaging -3.73% before \sim 8.6 ka BP, and then declining to -5.89% following \sim 8.6 ka BP.

For the overlapping time period (7.25–8.49 ka BP), the δ^{18} O value of Tetukhe-T1 (-9.5%) is 2.8% more negative than that of Sadovaya-S1 (-6.7%). In contrast, δ^{13} C values are similar, with Tetukhe-T1 at -6.6% and Sadovaya-S1 at -5.9%. This large δ^{18} O difference is notable, especially considering the proximity of the two caves (25 km apart) and their similar elevations.

We propose two potential reasons for this discrepancy: (a) *Mixing of seasonal precipitation*. In Tetukhe Cave, the thicker roof (>20 m) likely enhances the mixing of annual precipitation, particularly with winter vapor, which is characterized by significantly lower δ^{18} O values due to colder atmospheric conditions. This results in a more negative δ^{18} O signature in the speleothem records. In contrast, Sadovaya Cave, with a thinner roof (~10–12 m), experiences less mixing of seasonal waters, leading to relatively enriched δ^{18} O values in the cave deposits. (b) *Soil/Epikarst Evaporation*. Evaporation in the soil or epikarst zone may enrich δ^{18} O in dripwater. At Sadovaya Cave, shallower infiltration pathways (potentially linked to thinner roof or sparser vegetation) could enhance evaporation, enriching δ^{18} O values. This process preferentially affects oxygen isotopes due to kinetic fractionation during water evaporation, explaining the similar δ^{13} C values between caves (-6.6% vs. -5.9%). Considering our δ^{18} O records show great similarity with those from Japan (Mori et al., 2018) and South Korea (Jo et al., 2011) (which we discuss in further detail in Section 4.1), all exhibiting a notable negative shift between 8 and 9 ka BP, we infer evaporation only modifies local δ^{18} O baselines but not climate-driven signals. This aligns with the Hendy test, which indicates stable isotopic fractionation conditions (here stable disequilibrium) during deposition.

These factors influence only the local $\delta^{18}O$ values. We suggest that on millennial timescales, both caves reflect the same climate signals, as indicated by the relatively consistent patterns and fluctuations in $\delta^{13}C$ and $\delta^{18}O$ values during the overlapping period (Figure S3 in Supporting Information S1). However, further detailed comparison of the two $\delta^{18}O$ time series is challenging due to age model uncertainties and differences in temporal resolution. This similarity suggests that both records can be combined to reconstruct large-scale climate changes. Therefore, in the following discussion, we combine the isotopic records from the two caves to better represent regional climate variability.

4. Discussion

4.1. Moisture Sources Changes Indicated by Speleothem δ^{18} O

High-resolution speleothem δ^{18} O, inherited from atmospheric precipitation, effectively captures the monsoon variability on multiple timescales (Cheng et al., 2022). In EASM regions, upstream isotope depletion recorded in speleothem δ^{18} O records is primarily due to monsoon circulation intensity (or spatial-scales) and the associated rainout effect along the moisture trajectory, as noted in previous model studies (Liu et al., 2014; Pausata et al., 2011). High δ^{18} O values indicate weakened summer monsoon dynamics or circulation, while low δ^{18} O values suggest strengthened monsoon dynamics on a wide range of timescales (Cheng et al., 2012, 2022; H. Zhang et al., 2021; Zhao et al., 2023). However, given the region's complex topography and climate conditions, there is no consensus yet on the interpretation of speleothem δ^{18} O in Northeast Asia, with existing interpretations including

WANG ET AL. 4 of 13

EASM intensity (Jo et al., 2011), the East Asian winter monsoon (Sone et al., 2013), seawater $\delta^{18}O$ (Mori et al., 2018), or temperature (Kano et al., 2023; Kato et al., 2023) changes. Our preliminary analysis of precipitation and oxygen isotope data reveals pronounced seasonal rainfall concentration, with 40%–65% of annual precipitation occurring during summer months. Considering this region's unique geographical position, we investigate moisture sources as a potential modulator of $\delta^{18}O$ variability. Using IsoGSM2 tagging simulations (Yoshimura et al., 2008), we quantified moisture contributions from the Pacific Ocean (PCO), terrestrial sources (LAND), and the Indian Ocean (IO). Seasonal analyses demonstrate that precipitation $\delta^{18}O$ becomes progressively depleted as summer rainfall intensifies (Figure 1d), yet this depletion is asynchronous with shifts in moisture sources (Figures S4a and S4c in Supporting Information S1). This negative $\delta^{18}O$ -precipitation correlation is corroborated by modern observations from six nearby GNIP stations (Figure 1c). Similarly, interannual $\delta^{18}O$ variations exhibit significant negative correlations with summer (JJAS) rainfall but no clear linkage to moisture source changes (Figures S4b, S4d, and S5 in Supporting Information S1), aligning with patterns observed across East Asia.

However, some studies show that on orbital timescales, more pronounced changes in monsoon circulation due to insolation forcing may effectively shift both distant and nearby moisture sources, further altering $\delta^{18}O$ signals (Q. Wen et al., 2024). Our IsoGSM2 simulations reveal that the moisture source for North China and Northeast Asia differs significantly (Figure S6 in Supporting Information S1): Continental sources dominate North China (~70%), while Pacific-derived moisture accounts for nearly one-third of Northeast Asia's supply. Pacific Ocean moisture is generally more depleted in ^{18}O (Xue et al., 2023), partly due to secondary evaporation processes beneath the cloud layer, which leads to the enrichment of ^{18}O in the resultant water vapor and precipitation (Tang et al., 2015). Additionally, inland moisture does not always contribute to precipitation during transport, resulting in less depletion of heavy isotopes. In contrast, oceanic moisture undergoes continuous condensation and precipitation along its transport path, causing a progressive depletion of heavy isotopes (Z. Cai & Tian, 2016; M. Tan, 2016; Xia et al., 2020). Consequently, an increased contribution of moisture from the PCO, which is relatively more depleted in ^{18}O compared to continental moisture, would lead to more negative $\delta^{18}O$ values in both meteoric and speleothem records. Based on this, we suggest that $\delta^{18}O$ in Northeast Asia reflects changes in contribution of moisture sources, particularly the moisture fraction from the PCO on longer time-scales. However, this hypothesis requires further study through both reconstructions and model simulations in future.

Our speleothem $\delta^{18}O$ records from the Russian Far East reveal a notable negative shift between 8 and 9 ka BP, which are also evident in $\delta^{18}O$ records from Japan (Mori et al., 2018) and South Korea (Jo et al., 2011) (Figure 2). This suggests that climate changes in Northeast Asia exhibit strong spatial consistency on a large area. This contrasts with the $\delta^{18}O$ increase observed in North China (Zhenzhu Cave) (Y. Li et al., 2020) and the core monsoon regions, such as the Dongge Cave record (Dykoski et al., 2005; Y. Wang et al., 2005) (Figure 2). This discrepancy highlights the heterogeneous response between the EASM rainfall over the northeastern margin of Asia and North China during the early Holocene. The decrease in $\delta^{18}O$ values in Northeast Asia between \sim 8 and 9 ka may suggest an increased contribution of moisture from the Pacific, a hypothesis that will be further discussed in subsequent sections.

4.2. Regional Precipitation Change Indicated by δ^{13} C

The δ^{13} C values in cave deposits are influenced by multiple processes, including: changes in cave ventilation and water-rock interaction, prior carbonate precipitation (PCP) in the vadose zone, and the type of vegetation and the soil process above the cave (Genty et al., 2001). Typically, under dry conditions, slower water discharge would increase water-rock interaction time, enhancing both carbonate dissolution from bedrock and PCP process in the vadose zone (Fairchild et al., 2006; Johnson et al., 2006). These processes collectively enrich δ^{13} C values in drip water and speleothems. The δ^{13} C values are also influenced by the type of vegetation and the process in soil above the cave, which are in turn affected by external hydrological conditions (L. Tan et al., 2020). On the one hand, variations in δ^{13} C value can reflect vegetation type with different photosynthetic pathways (McDermott, 2004) above the cave system, which respond differently to changes in temperature, humidity, and atmospheric CO₂ concentrations (Coplen et al., 1994; Dorale et al., 1992; Genty et al., 2001). Evidence suggests that the vegetation around Vladivostok is predominantly C3-type, corresponding with the temperate climate of the region (Mokhova et al., 2009). Since the δ^{13} C values of modern C3 vegetation have a significant negative correlation with mean annual precipitation (r = -0.43 (Rao et al., 2017)), it is expected that drier conditions would lead to heavier δ^{13} C values in both vegetation and speleothems. On the other hand, reduced vegetation density under drier conditions

WANG ET AL. 5 of 13

194807, 2023, 20, Downloaded from https://agupubs.on.inleibtarry.wiley.com/doi/0.1029/2025GL114717 by British Attactic Survey, Wiley Online Library on [16/1/0.205]. See the Terms and Conditions (https://onlinelibrary.wiley.com/terms-and-conditions) on Wiley Online Library for takes of use; OA articles are governed by the applicable Creat

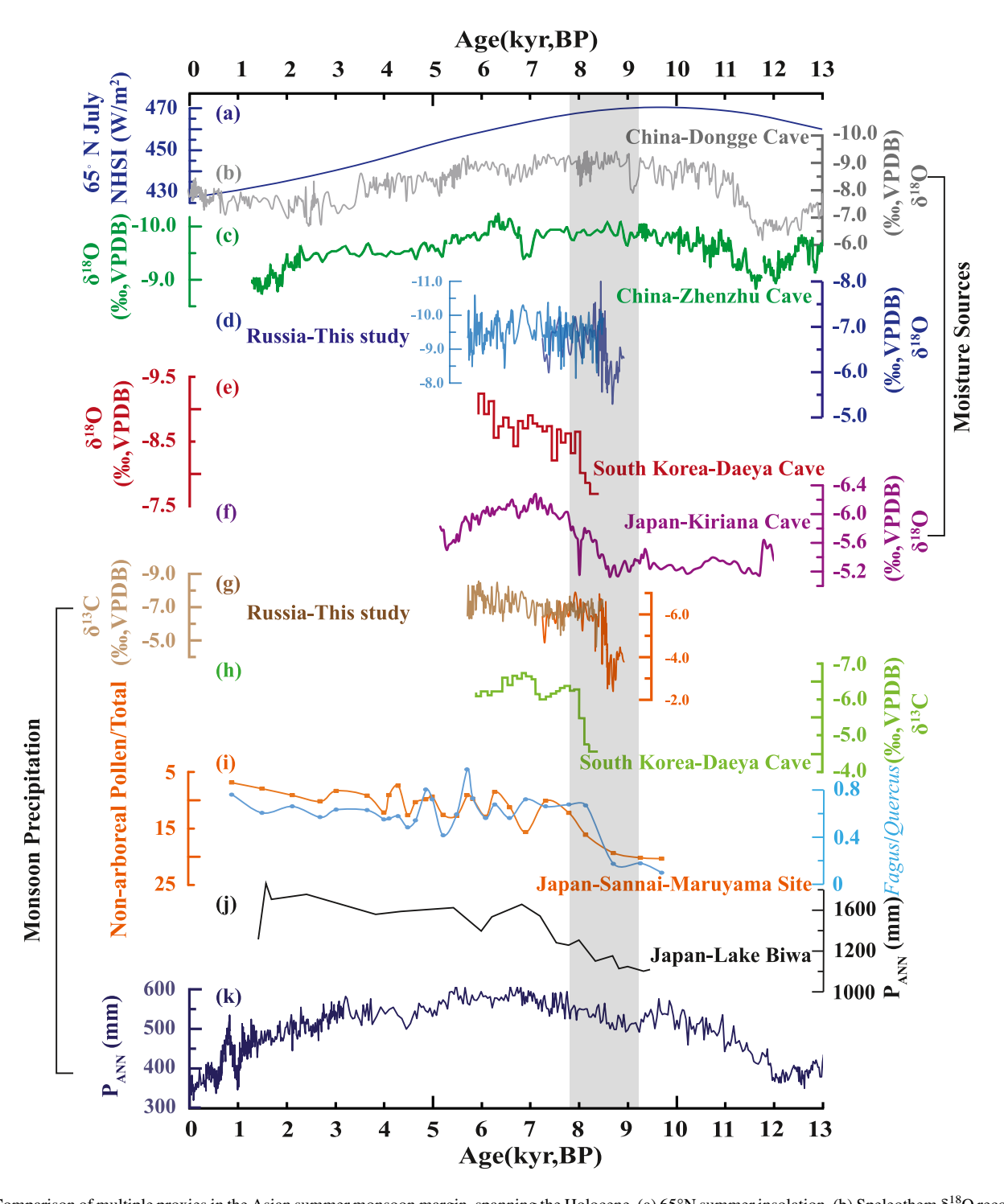


Figure 2. Comparison of multiple proxies in the Asian summer monsoon margin, spanning the Holocene. (a) 65°N summer insolation. (b) Speleothem $\delta^{18}O$ records from Dongge Cave, southern China (Dykoski et al., 2005; Y. Wang et al., 2005). (c) Speleothem $\delta^{18}O$ records from Zhenzhu Cave, northern China (Y. Li et al., 2020). (d) Speleothem $\delta^{18}O$ records in this study. (e) Daeya cave speleothem $\delta^{18}O$ records from South Korea (Jo et al., 2011). (f) Kiriana cave speleothem $\delta^{18}O$ records (Mori et al., 2018) from Japan. (g) Speleothem $\delta^{13}C$ records in this study. (h) Daeya cave speleothem $\delta^{13}C$ records from South Korea (Jo et al., 2011). (i) Pollen-based proxies from the Sanai-Maruyama Site, Japan: the ratio of Fagus to Quercus subgen. Lepidobalanus pollen, and the proportion of non-arboreal pollen to total pollen (Kawahata et al., 2009). (j) Pollen-based annual precipitation reconstructed from Lake Biwa, Japan (Kigoshi et al., 2014). (k) Pollen-based annual precipitation reconstructed from Gonghai Lake, northern China (Chen et al., 2015). The gray shadow indicates the significant change between 8 and 9 ka.

WANG ET AL. 6 of 13

can decrease plant root respiration and lower the organic matter content in the soil. This results in less CO_2 being produced by soil microorganisms, leading to heavier $\delta^{13}C$ values in drip water and speleothems (L. Tan et al., 2020). Collectively, arid conditions can prolong water-rock interaction, enhance PCP, diminish vegetation cover, and reduce microbial activity in the soil above the cave, ultimately leading to elevated $\delta^{13}C$ values, vice versa (Pérez-Mejías et al., 2019).

Therefore, the pronounced negative shift in $\delta^{13}C$ around 8.6 ka BP indicates a regional transition to a more humid climate at that time. This finding is consistent with records from Japan (Kawahata et al., 2009; Kigoshi et al., 2014) and South Korea (Jo et al., 2011) (Figure 2). Moreover, speleothems in both Sadovaya Cave and Daeya Cave began to grow between 8 and 9 ka BP. Speleothem formation depends on the availability of infiltrating water, which supplies dissolved calcium carbonate and facilitates carbonate deposition through CO_2 degassing. In karst systems, the initiation of speleothem growth is typically interpreted as a shift toward wetter environmental conditions. Therefore, for the relatively arid Northeast Asia, the synchronous inceptive growths of speleothems in Sadovaya Cave and Daeya Cave likely signifies a transition to more humid conditions during the time. Taken together, multiple lines of evidence suggest an increase in precipitation across Northeast Asia since 8.2–8.6 ka BP, or perhaps even earlier.

4.3. Driving Mechanism for Precipitation and Circulation Changes in the Early-Mid Holocene

Our study reveals a significant negative δ^{18} O shift and intensified monsoon precipitation in Northeast Asia between 8 and 9 ka BP, in contrast to the patterns observed in North China (Figure 2). From a spatial perspective (Figure 3), the negative δ^{18} O shift from 9 to 6 ka aligns with changes observed in the Nuanhuo Cave record in Northeast China (Wu et al., 2012), as well as Shennong and Xianyun cave records in Southeast China (H. Zhang et al., 2021). In contrast, it differs from most other speleothem δ^{18} O records from Southwest and North China (Y. Cai et al., 2010, 2021; Dong et al., 2015; Dykoski et al., 2005; Y. Li et al., 2020; H.-L. Zhang et al., 2013), as well as South Asia (Kathayat et al., 2016). Meanwhile, the increased precipitation from 9 to 6 ka corresponds to patterns observed in southern China (W. Zhang et al., 2018; H. Zhang et al., 2021; Zheng et al., 2020; Zhu et al., 2010) but contrasts with reductions in northern China and South Asia (Cao et al., 2010; Cheddadi, 2020; Goldsmith et al., 2017; Hong et al., 2005; Lauterbach et al., 2020; G. Li et al., 2020; Ming et al., 2020; Zhong et al., 2015). These spatial variations align closely with the differences in JJAS and annual precipitation δ^{18} O and amounts between 9 and 6 ka BP simulated by the COSMOS-wiso isotope-enabled climate model (H. Zhang et al., 2021) (Figure 3, detailed information of COSMOS-wiso can be found in Text S1 in Supporting Information S1). The model further illustrates contrasting responses of precipitation monsoon rainfall and oxygen isotopes between Northeast Asia and the coastal regions compared to the expansive inner continental regions. Since these time-slice experiments at 9 and 6 ka are mainly driven by corresponding orbital parameters while maintaining other boundary conditions identical to the pre-industrial period, the results suggest that the distinct patterns of δ^{18} O and rainfall are inherent features of monsoon variability, which are primarily controlled by orbital forcing. This is basically consistent with the notion of the "monsoon system sciences," underlining a systematic/integrative view of different dynamic natures/responses/feedback across an exceptionally broad range of temporospatial scales in a monsoon system and put them into the context of external insolation and internal (ice volume/CO₂) forcings (Cheng et al., 2021, 2022).

Although the speleothem records around Northeast Asia are relatively short, making it challenging to definitively conclude how $\delta^{18}O$ and rainfall evolved throughout the Holocene, two longer pollen records from Japan provide additional insights (Kawahata et al., 2009; Kigoshi et al., 2014). These records indicate that regional rainfall increased since the early Holocene, even as NHSI decreased (Figures 2i and 2j). This contrasts with decreased precipitation observed in North China, such as in the Gonghai Lake record (Chen et al., 2015) (Figure 2k). Such discrepancies suggest that the dipole response between Northeast Asia and North China may persist on longer timescales. This contrasting pattern aligns with the "dipole pattern" observed between land and ocean, as revealed by numerous previous climate simulations (Jalihal et al., 2019). Furthermore, it supports recent modeling studies that demonstrate a grand dipole response of rainfall oxygen isotope and amount among South Asia, North China, and Japan to the orbital forcing (Q. Wen et al., 2024).

Regarding the precipitation change, the decrease in NHSI from 9 to 6 ka BP, or from the early to late Holocene, led to a reduction in the land-sea temperature contrast in summertime, which in turn weakened the southwesterly wind (H. Zhang et al., 2021) (Figures 3c and 3d). Simultaneously, a weakened WPSH and southward shift of the westerly jet (evidenced in circulation change at multiple level, Figure S7 in Supporting Information S1)- were

WANG ET AL. 7 of 13

1944807, 2025, 20, Dowloaded from https://agupubs.onlinelibrary.wiley.com/doi/10.1029/2025GL114717 by British Antarctic Survey, Wiley Online Library on [16/10/2025]. See the Terms and Conditions (https://onlinelibrary.wiley

and-conditions) on Wiley Online Library for rules of use; OA articles are governed by the applicable Creat

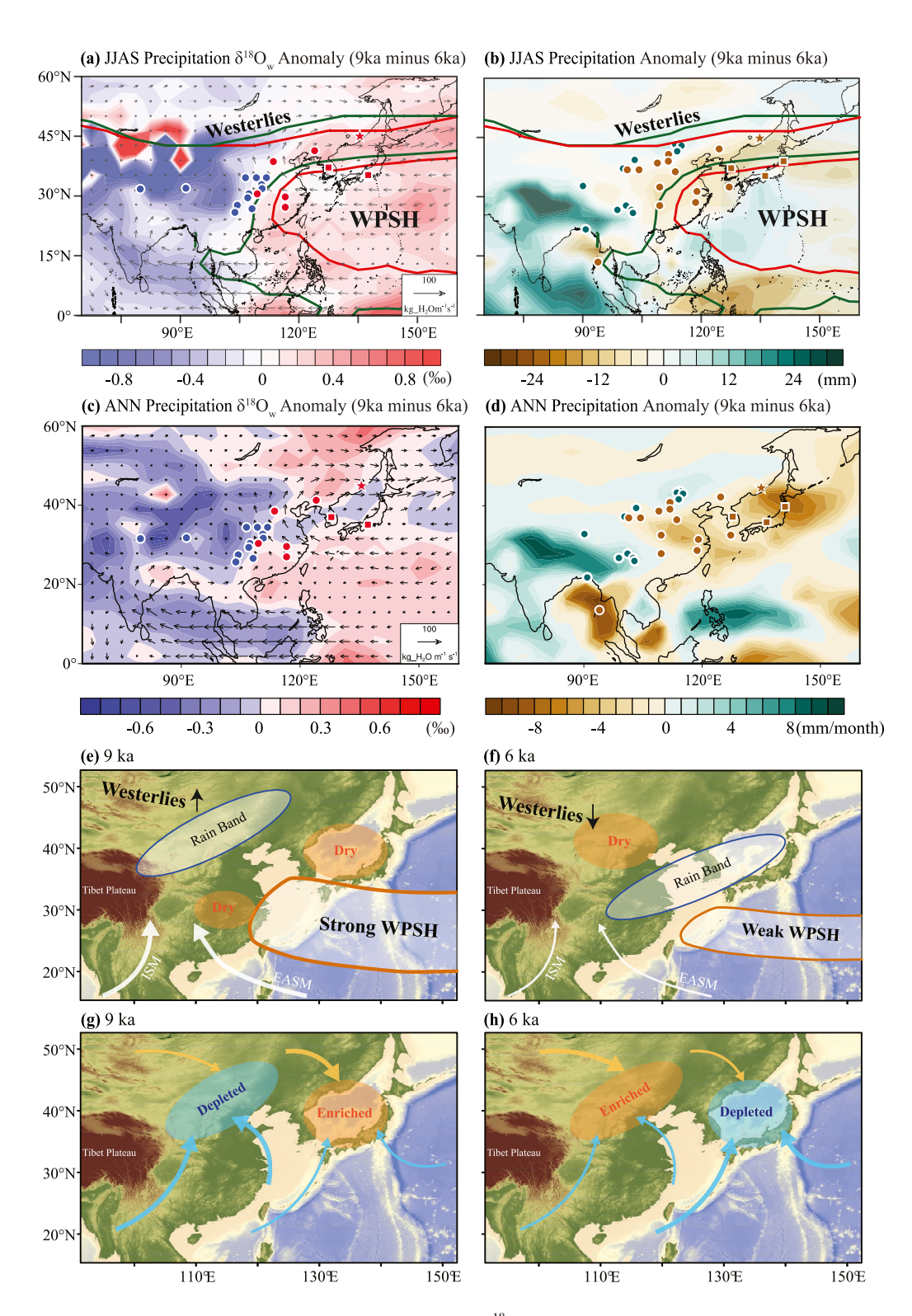


Figure 3. Simulated and schematic changes in precipitation amount and precipitation $\delta^{18}O$ between 9 and 6 ka. (a–d) Simulated differences (9 kyr minus 6 kyr) in June–July–August–September (JJAS) and annual precipitation $\delta^{18}O$ (a, c, shade) and precipitation amount (b, d, shade) from the isotope-enabled general circulation model COSMOS-wiso (modified from H. Zhang et al. (2021)). Shading indicates the magnitude of anomalies; arrows represent JJA 850-hPa water vapor transport. The circle dots denote sites from original literature, while the squares and pentagons are new points added in this study (see Figure 1a for locations). The filled colors of these points are qualitatively comparable to the anomaly color bars. (e–h) Schematic diagrams illustrating precipitation (e, f) and $\delta^{18}O$ (g, h) variations at 9 and 6 ka. Blue arrows indicate water vapor originating from the Indian Ocean and Pacific Ocean, while orange arrows represent water vapor coming from the land.

WANG ET AL. 8 of 13

driven by reduced zonal asymmetric diabatic heating and enhanced meridional temperature gradient. These changes displaced the East Asian moisture front southward (Q. Wen et al., 2024), generating a rainfall dipole pattern: reduced precipitation over North China versus increased rainfall across South China and Japan. This paleorainfall pattern appears mechanistically analogous to modern seasonal rainband displacements driven by insolation-forced oscillations of the westerly jet and western Pacific subtropical high (WPSH). From May and June to July and August, the WPSH intensifies and shifts northward, while the westerly jet axis migrates \sim 2°N poleward (Figure 1a). This coupled intensification of the WPSH and northward displacement of the jet drives the East Asian rainbelt northward, enhancing precipitation over northern China while reducing rainfall across southeastern China and southern Japan (Z. Li et al., 2024; Y. Wang et al., 2023). Conversely, when the WPSH weakens and westerly jet shifts southward (equivalent to the period from July-August to May-June, Figure 1a), the rainbelt retreats southward, creating a distinct belt of increased precipitation from southeastern China to southern Japan.

Although this modern precipitation belts rarely extend into Northeast Asia, stronger early Holocene insolation likely amplified the western Pacific subtropical high (WPSH) intensity and shifted the westerly jet poleward. These circulation modifications could have extended precipitation influence over wider areas—including Northeast Asia—more significantly than today. This interpretation gains support from X. Li et al.'s (2021) analysis of modern circulation variability on interannual scale: during anti-phase WPSH-jet configurations (characterized by WPSH weakening and southward jet displacement), coherent wet anomalies emerge across the Yangtze River basin, southern Japan, and the Korean Peninsula while North China experiences drying—precisely mirroring the 9–6 ka BP dipole pattern identified in our study. This consistency further underscores the combined role of WPSH and westerly jet dynamics in generating continental-scale precipitation dipoles.

As to δ^{18} O changes, it is suggested that orbital-scale δ^{18} O variations over the ASM region are primarily driven by changes in the relative contributions of moistures from different source regions, with more distant sources contributing to more negative δ^{18} O_p, and vice versa (Kong et al., 2017; Q. Wen et al., 2024). Our moisture analysis reveals distinct differences in moisture sources between Northeast Asia and North China. For Northeast Asia, the contribution from the Asian continent is relatively low compared to North China with approximately 70% of the moisture coming from the continent. In contrast, the PCO plays a much greater role in Northeast Asia, contributing nearly a third of the total moisture. As NHSI decreased from 9 to 6 ka, the weakening of the southwesterly monsoon wind, coupled with the southward shift of the Meiyu-Baiu rainbelt, reduced the contribution of PCO moisture to North China, resulting in the δ^{18} O increase. Meanwhile, the relative contribution of the nearby PCO moisture to Northeast Asia increased, leading to the δ^{18} O decrease in that region (Figures 3e and 3f).

Overall, both monsoon rainfall and speleothem δ^{18} O exhibit contrasting patterns between Northeast Asia and North China during the early to mid-Holocene, highlighting the diverse responses of rainfall and δ^{18} O to NHSI forcing. These contrasting patterns are further supported by the diverse patterns observed across eastern China during the Holocene (H. Zhang et al., 2021). Some studies suggest that variations in ice volume may have shifted the rainfall maximum in Northern China from the Early to Middle Holocene by influencing CO₂ concentrations (Lu et al., 2013) or the AMOC (Chen et al., 2015). However, modeling results indicate that remnant ice sheets over North America during the Early Holocene likely had negligible impacts on atmospheric circulation in remote East Asia (Gregoire et al., 2018; Jin et al., 2012; Weber & Tuenter, 2011). Our findings emphasize that the unique patterns of δ^{18} O and rainfall are fundamental characteristics of monsoon system, primarily controlled by NSHI. The internal processes, such as ice sheet melting and vegetation feedback, may have secondary effects, either amplifying or dampening these variations. The phase differences between speleothem isotope records and other moisture proxies align broadly with the dynamics of monsoon systems under the NHSI forcing. Notably, the abrupt δ^{18} O/precipitation shift at ~9-8 ka may present an intriguing nonlinear response to gradual insolation change. We cautiously propose this may parallel modern intraseasonal thresholds where the WPSH exhibits abrupt northward jumps (mid-June and mid-July), corresponding to the EASM's characteristic three quasistationary stages separated by two rapid transitions (Ding & Chan, 2005). Though orbital and seasonal timescales differ, similar atmospheric reorganization mechanisms—potentially involving coupled WPSH-jet displacements—might operate across timescales. This hypothesis requires further validation through dedicated modeling studies.

WANG ET AL. 9 of 13

19448007, 2025, 20, Downloaded from https:/

doi/10.1029/2025GL114717 by British Antarctic Survey, Wiley Online Library on [16/10/2025]. See the Terms and Cond

5. Conclusions

We conducted a comprehensive analysis on new $\delta^{18}O$ and $\delta^{13}C$ records from two speleothems from the Russian Far East, spanning 9 to 5 ka BP, which represent the northernmost cave records thus far in the EASM region. This study, in conjunction with other records from Northeast Asia, indicates a significant synchronous negative shift of the speleothem $\delta^{18}O$ and intensified monsoon precipitation in Northeast Asia between 8 and 9 ka BP, contrasting with the rainfall and speleothem $\delta^{18}O$ patterns observed in North China. We suggest that this contrasting pattern may be driven by changes in NHSI during the Holocene. A decrease in NHSI would weaken the southwesterly winds and the WPSH, while simultaneously inducing a southward shift of the westerly jet. These changes collectively force the rain belt southward, thereby reducing precipitation in North China while increasing it in Northeast Asia. Additionally, this shift would reduce (increase) the contribution of the PCO moisture to North China (Northeast Asia), resulting in $\delta^{18}O$ increase (decrease). In summary, our study sheds light on the complex evolution of the precipitation and $\delta^{18}O$ in Northeast Asia, emphasizing the pivotal role of NHSI in driving monsoon climate dynamics.

Conflict of Interest

The authors declare no conflicts of interest relevant to this study.

Data Availability Statement

The Supporting Information S1 and Table S1 are available through Zenodo (Wang et al., 2025). The Table S1 in Supporting Information S1 includes the carbon and oxygen isotope data. The Supporting Information S1 includes a pdf file contains Text S1 for details on the climate model, Text S2 for details on the methods of all the lab work, Figure S1 for age models, Figure S2 for the results of the Hendy test, Figure S3 for the results of Tetukhe-T1 and Sadovaya-S1 speleothem records, Figure S4 for the relationship between moisture source and regional δ^{18} O, Figure S5 for the relationship between regional precipitation and δ^{18} O, Figure S6 for the moisture source analyses for North China and Northeast Asia, Figure S7 for the vertical Structure of Wind Fields During Mid-Holocene (6 ka) and Early Holocene (9 ka), Figure S8 for the comparison of δ^{18} O values, precipitation from the isoGSM model, and GNIP Terney station (1996–2000), Table S1 for the 230 Th dating results, Table S2 in Supporting Information S1 for experiment details performed in COSMOS-wiso.

Acknowledgments

The authors would like to thank
Dr. Jingjing Wang and Jiayu Lu from
Yancheng Teachers University, Xinyu Li
from Hohai University for their assistance
with climate data modeling and analysis.
This study is supported by grants from
National Natural Science Foundation of
China (NSFC 42488201, 42302118,
42261144753) and the Russian state
budget (number 121021700342-9 of the
POI FEB RAS).

References

- Belyanin, P., & Belyanina, N. (2021). The late Pleistocene and Holocene history of Pinus koraiensis (Korean Pine) in the south of the Russian Far East based on palynological data. *Acta Palaeobotanica*, 61(2), 148–170. https://doi.org/10.35535/acpa-2021-0010
- Cai, Y., Cheng, X., Ma, L., Mao, R., Breitenbach, S. F. M., Zhang, H., et al. (2021). Holocene variability of East Asian summer monsoon as viewed from the speleothem δ¹⁸O records in central China. Earth and Planetary Science Letters, 558, 116758. https://doi.org/10.1016/j.epsl. 2021.116758
- Cai, Y., Fung, I. Y., Edwards, R. L., An, Z., Cheng, H., Lee, J. E., et al. (2015). Variability of stalagmite-inferred Indian monsoon precipitation over the past 252,000 y. Proceedings of the National Academy of Sciences, 112(10), 2954–2959. https://doi.org/10.1073/pnas.1424035112
- Cai, Y., Tan, L., Cheng, H., An, Z., Edwards, R. L., Kelly, M. J., et al. (2010). The variation of summer monsoon precipitation in central China since the last deglaciation. *Earth and Planetary Science Letters*, 291(1), 21–31. https://doi.org/10.1016/j.epsl.2009.12.039
- Cai, Z., & Tian, L. (2016). Atmospheric controls on seasonal and interannual variations in the precipitation isotope in the East Asian Monsoon Region. *Journal of Climate*, 29(4), 1339–1352. https://doi.org/10.1175/JCLI-D-15-0363.1
- Cao, X., Xu, Q., Jing, Z., Tang, J., Li, Y., & Tian, F. (2010). Holocene climate change and human impacts implied from the pollen records in Anyang, central China. *Quaternary International*, 227(1), 3–9. https://doi.org/10.1016/j.quaint.2010.03.019
- Cheddadi, R. (2020). How the Asian subtropical area became evergreen since the Last Glacial Maximum. Past Global Changes Magazine, 28(1). https://doi.org/10.22498/pages.28.1.6
- Chen, F., Xu, Q., Chen, J., Birks, H. J. B., Liu, J., Zhang, S., et al. (2015). East Asian summer monsoon precipitation variability since the last deglaciation. *Scientific Reports*, 5(1), 11186. https://doi.org/10.1038/srep11186
- Cheng, H., Edwards, R. L., Sinha, A., Spötl, C., Yi, L., Chen, S., et al. (2016). The Asian monsoon over the past 640,000 years and ice age terminations. *Nature*, 534(7609), 640–646. https://doi.org/10.1038/nature18591
- Cheng, H., Edwards, R. L., Wang, Y., Kong, X., Ming, Y., Kelly, M. J., et al. (2006). A penultimate glacial monsoon record from Hulu Cave and two-phase glacial terminations. *Geology*, 34(3), 217. https://doi.org/10.1130/g22289.1
- Cheng, H., Fleitmann, D., Edwards, R. L., Wang, X., Cruz, F. W., Auler, A. S., et al. (2009). Timing and structure of the 8.2 kyr B.P. event inferred from δ¹⁸O records of stalagmites from China, Oman, and Brazil. *Geology*, 37(11), 1007–1010. https://doi.org/10.1130/g30126a.1
- Cheng, H., Li, H., Sha, L., Sinha, A., Shi, Z., Yin, Q., et al. (2022). Milankovitch theory and monsoon. *The Innovation*, 3(6), 100338. https://doi.org/10.1016/j.xinn.2022.100338
- Cheng, H., Sinha, A., Wang, X., Cruz, F. W., & Edwards, R. L. (2012). The Global Paleomonsoon as seen through speleothem records from Asia and the Americas. *Climate Dynamics*, 39(5), 1045–1062. https://doi.org/10.1007/s00382-012-1363-7
- Cheng, H., Zhang, H., Cai, Y., Shi, Z., Yi, L., Deng, C., et al. (2021). Orbital-scale Asian summer monsoon variations: Paradox and exploration. Science China Earth Sciences, 64(4), 529–544. https://doi.org/10.1007/s11430-020-9720-y

WANG ET AL. 10 of 13

- Cheng, H., Zhang, H., Zhao, J., Li, H., Ning, Y., & Kathayat, G. (2019). Chinese stalagmite paleoclimate researches: A review and perspective. Science China Earth Sciences, 62(10), 1489–1513. https://doi.org/10.1007/s11430-019-9478-3
- Coplen, T. B., Winograd, I. J., Landwehr, J. M., & Riggs, A. C. (1994). 500,000-Year stable carbon isotopic record from Devils Hole, Nevada. Science, 263(5145), 361–365, https://doi.org/10.1126/science.263.5145.361
- Ding, Y., & Chan, J. C. L. (2005). The East Asian summer monsoon: An overview. *Meteorology and Atmospheric Physics*, 89(1–2), 117–142. https://doi.org/10.1007/s00703-005-0125-z
- Dong, J., Shen, C.-C., Kong, X., Wang, H.-C., & Jiang, X. (2015). Reconciliation of hydroclimate sequences from the Chinese Loess Plateau and low-latitude East Asian Summer Monsoon regions over the past 14,500 years. *Palaeogeography, Palaeoclimatology, Palaeoecology*, 435, 127–135. https://doi.org/10.1016/j.palaeo.2015.06.013
- Dorale, J. A., González, L. A., Reagan, M. K., Pickett, D. A., Murrell, M. T., & Baker, R. G. (1992). A high-resolution record of Holocene climate change in speleothem calcite from Cold Water Cave, Northeast Iowa. *Science*, 258(5088), 1626–1630. https://doi.org/10.1126/science.258. 5088,1626
- Dykoski, C. A., Edwards, R. L., Cheng, H., Yuan, D., Cai, Y., Zhang, M., et al. (2005). A high-resolution, absolute-dated Holocene and deglacial Asian monsoon record from Dongge Cave, China. *Earth and Planetary Science Letters*, 233(1–2), 71–86. https://doi.org/10.1016/j.epsl.2005. 01.036
- Fairchild, I. J., Smith, C. L., Baker, A., Fuller, L., Spötl, C., Mattey, D., et al. (2006). Modification and preservation of environmental signals in speleothems. *Earth-Science Reviews*, 75(1), 105–153. https://doi.org/10.1016/j.earscirev.2005.08.003
- Genty, D., Baker, A., Massault, M., Proctor, C., Gilmour, M., Pons-Branchu, E., & Hamelin, B. (2001). Dead carbon in stalagmites: Carbonate bedrock paleodissolution vs. ageing of soil organic matter. Implications for 13C variations in speleothems. *Geochimica et Cosmochimica Acta*, 65(20), 3443–3457. https://doi.org/10.1016/S0016-7037(01)00697-4
- Goldsmith, Y., Broecker, W. S., Xu, H., Polissar, P. J., de Menocal, P. B., Porat, N., et al. (2017). Northward extent of East Asian monsoon covaries with intensity on orbital and millennial timescales. *Proceedings of the National Academy of Sciences*, 114(8), 1817–1821. https://doi.org/10.1073/pnas.1616708114
- Gregoire, L. J., Ivanovic, R. F., Maycock, A. C., Valdes, P. J., & Stevenson, S. (2018). Holocene lowering of the Laurentide ice sheet affects North Atlantic gyre circulation and climate. Climate Dynamics, 51(9), 3797–3813. https://doi.org/10.1007/s00382-018-4111-9
- Hendy, C. H., & Wilson, A. T. (1968). Palaeoclimatic data from speleothems. *Nature*, 219(5149), 48–51. https://doi.org/10.1038/219048a0
- Hong, Y. T., Hong, B., Lin, Q. H., Shibata, Y., Hirota, M., Zhu, Y. X., et al. (2005). Inverse phase oscillations between the East Asian and Indian Ocean summer monsoons during the last 12000 years and paleo-El Niño. Earth and Planetary Science Letters, 231(3), 337–346. https://doi.org/ 10.1016/j.epsl.2004.12.025
- Jalihal, C., Srinivasan, J., & Chakraborty, A. (2019). Modulation of Indian monsoon by water vapor and cloud feedback over the past 22,000 years. Nature Communications, 10(5701), 5701. https://doi.org/10.1038/s41467-019-13754-6
- Jin, L., Chen, F., Morrill, C., Otto-Bliesner, B. L., & Rosenbloom, N. (2012). Causes of early Holocene desertification in arid central Asia. Climate Dynamics, 38(7), 1577–1591. https://doi.org/10.1007/s00382-011-1086-1
- Jo, K.-N., Woo, K. S., Lim, H. S., Cheng, H., Edwards, R. L., Wang, Y., et al. (2011). Holocene and Eemian climatic optima in the Korean Peninsula based on textural and carbon isotopic records from the stalagmite of the Daeya Cave, South Korea. *Quaternary Science Reviews*, 30(9-10), 1218-1231. https://doi.org/10.1016/j.quascirev.2011.02.012
- Johnson, K. R., Hu, C., Belshaw, N. S., & Henderson, G. M. (2006). Seasonal trace-element and stable-isotope variations in a Chinese speleothem: The potential for high-resolution paleomonsoon reconstruction. *Earth and Planetary Science Letters*, 244(1–2), 394–407. https://doi.org/10.1016/j.epsl.2006.01.064
- Kano, A., Kato, H., & Murata, A. (2023). Oxygen isotopes of the Japanese stalagmites as global and local paleoclimate proxies. *Island Arc*, 32(1), e12491. https://doi.org/10.1111/iar.12491
- Kathayat, G., Cheng, H., Sinha, A., Spotl, C., Edwards, R. L., Zhang, H., et al. (2016). Indian monsoon variability on millennial-orbital timescales. Scientific Reports, 6(1), 24374. https://doi.org/10.1038/srep24374
- Kato, H., Mori, T., Amekawa, S., Wu, C.-C., Shen, C.-C., & Kano, A. (2023). Coevolutions of terrestrial temperature and monsoonal precipitation amounts from the latest Pleistocene to the mid-Holocene in Japan: Carbonate clumped isotope record of a stalagmite. *Chemical Geology*, 622, 121390. https://doi.org/10.1016/j.chemgeo.2023.121390
- Kawahata, H., Yamamoto, H., Ohkushi, K. I., Yokoyama, Y., Kimoto, K., Ohshima, H., & Matsuzaki, H. (2009). Changes of environments and human activity at the Sannai-Maruyama ruins in Japan during the mid-Holocene Hypsithermal climatic interval. *Quaternary Science Reviews*, 28(9–10), 964–974. https://doi.org/10.1016/j.quascirev.2008.12.009
- Kigoshi, T., Kumon, F., Hayashi, R., Kuriyama, M., Yamada, K., & Takemura, K. (2014). Climate changes for the past 52 ka clarified by total organic carbon concentrations and pollen composition in Lake Biwa, Japan. *Quaternary International*, 333, 2–12. https://doi.org/10.1016/j.quaint.2014.04.028
- Kong, W., Swenson, L. M., & Chiang, J. C. (2017). Seasonal transitions and the westerly jet in the Holocene East Asian summer monsoon. *Journal of Climate*, 30(9), 3343–3365. https://doi.org/10.1175/JCLI-D-16-0087.1
- Lauterbach, S., Andersen, N., Wang, Y. V., Blanz, T., Larsen, T., & Schneider, R. R. (2020). An ~130 kyr record of surface water temperature and δ¹⁸O from the Northern Bay of Bengal: Investigating the linkage between Heinrich events and weak monsoon intervals in Asia. *Paleoceanography and Paleoclimatology*, 35(2), e2019PA003646. https://doi.org/10.1029/2019PA003646
- Li, G., Wang, Z., Zhao, W., Jin, M., Wang, X., Tao, S., et al. (2020). Quantitative precipitation reconstructions from Chagan Nur revealed lag response of East Asian summer monsoon precipitation to summer insolation during the Holocene in arid northern China. *Quaternary Science Reviews*, 239, 106365. https://doi.org/10.1016/j.quascirev.2020.106365
- Li, Q., Wu, H., Yu, Y., Sun, A., Marković, S. B., & Guo, Z. (2014). Reconstructed moisture evolution of the deserts in northern China since the last Glacial Maximum and its implications for the East Asian Summer Monsoon. *Global and Planetary Change*, 121, 101–112. https://doi.org/10.1016/j.gloplacha.2014.07.009
- Li, X., Lu, R., & Li, G. (2021). Different configurations of interannual variability of the western North Pacific subtropical high and East Asian westerly jet in summer. Advances in Atmospheric Sciences, 38(6), 931–942. https://doi.org/10.1007/s00376-021-0339-0
- Li, Y., Rao, Z., Xu, Q., Zhang, S., Liu, X., Wang, Z., et al. (2020). Inter-relationship and environmental significance of stalagmite δ¹³C and δ¹⁸O records from Zhenzhu Cave, north China, over the last 130 ka. Earth and Planetary Science Letters, 536, 116149. https://doi.org/10.1016/j.epsl. 2020.116149
- Li, Z., Ren, H.-L., Lu, M., & Zhou, F. (2024). Interannual variations of westward extension area of western Pacific subtropical high and its relationship with precipitation in East Asia. Atmospheric Research, 298, 107148. https://doi.org/10.1016/j.atmosres.2023.107148
- Liu, Z., Wen, X., Brady, E., Otto-Bliesner, B., Yu, G., Lu, H., et al. (2014). Chinese cave records and the East Asia Summer Monsoon. Quaternary Science Reviews, 83, 115–128. https://doi.org/10.1016/j.quascirev.2013.10.021

WANG ET AL. 11 of 13

- Lu, H., Miao, X., Zhou, Y., Mason, J., Swinehart, J., Zhang, J., et al. (2005). Late Quaternary aeolian activity in the Mu Us and Otindag dune fields (north China) and lagged response to insolation forcing. *Geophysical Research Letters*, 32(21), L21716. https://doi.org/10.1029/2005gl024560
 Lu, H. Yi, S., Liu, Z., Mason, I. A., Jiang, D., Cheng, I., et al. (2013). Variation of East Asian monsoon precipitation during the past 21 k.y. and
- Lu, H., Yi, S., Liu, Z., Mason, J. A., Jiang, D., Cheng, J., et al. (2013). Variation of East Asian monsoon precipitation during the past 21 k.y. and potential CO₂ forcing. *Geology*, 41(9), 1023–1026. https://doi.org/10.1130/G34488.1
- McDermott, F. (2004). Palaeo-climate reconstruction from stable isotope variations in speleothems: A review. *Quaternary Science Reviews*, 23(7), 901–918. https://doi.org/10.1016/j.quascirev.2003.06.021
- Ming, G., Zhou, W., Wang, H., Cheng, P., Shu, P., Xian, F., & Fu, Y. (2020). Moisture variations in Lacustrine—Eolian sequence from the Hunshandake sandy land associated with the East Asian Summer Monsoon changes since the late Pleistocene. *Quaternary Science Reviews*, 233, 106210. https://doi.org/10.1016/j.quascirev.2020.106210
- Mokhova, L., Tarasov, P., Bazarova, V., & Klimin, M. (2009). Quantitative biome reconstruction using modern and late Quaternary pollen data from the southern part of the Russian Far East. *Quaternary Science Reviews*, 28(25–26), 2913–2926. https://doi.org/10.1016/j.quascirev.2009. 07.018
- Mori, T., Kashiwagi, K., Amekawa, S., Kato, H., Okumura, T., Takashima, C., et al. (2018). Temperature and seawater isotopic controls on two stalagmite records since 83 ka from maritime Japan. Quaternary Science Reviews, 192, 47–58. https://doi.org/10.1016/j.quascirev.2018.05.024
- Pausata, F. S. R., Battisti, D. S., Nisancioglu, K. H., & Bitz, C. M. (2011). Chinese stalagmite δ¹⁸O controlled by changes in the Indian monsoon during a simulated Heinrich event. *Nature Geoscience*, 4(7), 474–480. https://doi.org/10.1038/ngeo1169
- Pérez-Mejías, C., Moreno, A., Sancho, C., Martín-García, R., Spötl, C., Cacho, I., et al. (2019). Orbital-to-millennial scale climate variability during Marine Isotope Stages 5 to 3 in northeast Iberia. *Quaternary Science Reviews*, 224, 105946. https://doi.org/10.1016/j.quascirev.2019. 105946
- Rao, Z., Guo, W., Cao, J., Shi, F., Jiang, H., & Li, C. (2017). Relationship between the stable carbon isotopic composition of modern plants and surface soils and climate: A global review. Earth-Science Reviews. 165, 110–119. https://doi.org/10.1016/j.earscirev.2016.12.007
- Scholz, D., & Hoffmann, D. L. (2011). StalAge—An algorithm designed for construction of speleothem age models. *Quaternary Geochronology*, 6(3), 369–382. https://doi.org/10.1016/j.quageo.2011.02.002
- Sone, T., Kano, A., Okumura, T., Kashiwagi, K., Hori, M., Jiang, X., & Shen, C.-C. (2013). Holocene stalagmite oxygen isotopic record from the Japan Sea side of the Japanese Islands, as a new proxy of the East Asian winter monsoon. *Quaternary Science Reviews*, 75, 150–160. https://doi.org/10.1016/j.quascirey.2013.06.019
- Tan, L., Liu, W., Wang, T., Cheng, P., Zang, J., Wang, X., et al. (2020). A multiple-proxy stalagmite record reveals historical deforestation in central Shandong, northern China. Science China Earth Sciences, 63(10), 1622–1632. https://doi.org/10.1007/s11430-019-9649-1
- Tan, M. (2016). Circulation background of climate patterns in the past millennium: Uncertainty analysis and re-reconstruction of ENSO-like state. Science China Earth Sciences, 59(6), 1225–1241. https://doi.org/10.1007/s11430-015-5256-6
- Tang, Y., Pang, H., Zhang, W., Li, Y., Wu, S., & Hou, S. (2015). Effects of changes in moisture source and the upstream rainout on stable isotopes in precipitation—A case study in Nanjing, eastern China. *Hydrology and Earth System Sciences*, 19(10), 4293–4306. https://doi.org/10.5194/hess-19-4293-2015
- Wang, H., Chen, J., Zhang, X., & Chen, F. (2014). Palaeosol development in the Chinese Loess Plateau as an indicator of the strength of the East Asian summer monsoon: Evidence for a mid-Holocene maximum. *Quaternary International*, 334–335, 155–164. https://doi.org/10.1016/j.guaint.2014.03.013
- Wang, K., Zhao, J., Cai, Y., Zhang, H., Li, H., Zhang, X., et al. (2025). Contrasting responses of monsoon rainfall and speleothem oxygen isotope between Northeast Asia and North China during the early-mid Holocene [Dataset]. Zenodo. https://doi.org/10.5281/zenodo.14741902
- Wang, Y., Cheng, H., Edwards, R. L., An, Z. S., Wu, J., Shen, C., & Dorale, J. (2001). A high-resolution absolute-dated late Pleistocene monsoon record from Hulu Cave, China. Science, 294(5550), 2345–2348. https://doi.org/10.1126/science.1064618
- Wang, Y., Cheng, H., Edwards, R. L., He, Y., Kong, X., An, Z., et al. (2005). The Holocene Asian monsoon: Links to solar changes and north Atlantic climate. Science, 308(5723), 854–857. https://doi.org/10.1126/science.1106296
- Wang, Y., Cheng, H., Edwards, R. L., Kong, X., Shao, X., Chen, S., et al. (2008). Millennial- and orbital-scale changes in the East Asian monsoon over the past 224,000 years. *Nature*, 451(7182), 1090–1093. https://doi.org/10.1038/nature06692
- Wang, Y., Hu, H., Ren, X., Yang, X. Q., & Mao, K. (2023). Significant northward jump of the Western Pacific subtropical high: The interannual variability and mechanisms. *Journal of Geophysical Research: Atmospheres*, 128(6), e2022JD037742. https://doi.org/10.1029/2022jd037742
- Weber, S. L., & Tuenter, E. (2011). The impact of varying ice sheets and greenhouse gases on the intensity and timing of boreal summer monsoons. *Quaternary Science Reviews*, 30(3), 469–479. https://doi.org/10.1016/j.quascirev.2010.12.009
- Wen, Q., Liu, Z., Jing, Z., Clemens, S. C., Wang, Y., Yan, M., et al. (2024). Grand dipole response of Asian summer monsoon to orbital forcing. npj Climate and Atmospheric Science, 7(1), 202. https://doi.org/10.1038/s41612-024-00749-4
- Wen, R., Xiao, J., Fan, J., Zhang, S., & Yamagata, H. (2017). Pollen evidence for a mid-Holocene East Asian summer monsoon maximum in northern China. *Quaternary Science Reviews*, 176, 29–35. https://doi.org/10.1016/j.quascirev.2017.10.008
- Wu, J. Y., Wang, Y. J., Cheng, H., Kong, X. G., & Liu, D. B. (2012). Stable isotope and trace element investigation of two contemporaneous annually-laminated stalagmites from northeastern China surrounding the "8.2 ka event". Climate of the Past, 8(5), 1497–1507. https://doi.org/ 10.5194/cp-8-1497-2012
- Xia, C., Liu, G., Chen, K., Hu, Y., Zhou, J., Liu, Y., & Mei, J. (2020). Stable isotope characteristics for precipitation events and their responses to moisture and environmental changes during the summer monsoon period in Southwestern China. *Polish Journal of Environmental Studies*, 29(3), 2429–2445. https://doi.org/10.15244/pjoes/110445
- Xu, Z., Mason, J. A., Xu, C., Yi, S., Bathiany, S., Yizhaq, H., et al. (2020). Critical transitions in Chinese dunes during the past 12,000 years. Science Advances, 6(9), eaay8020. https://doi.org/10.1126/sciady.aay8020
- Xue, Y.-X., Zhang, J., Su, Z., Wu, Y., Liang, Q.-S., Liang, M.-Q., et al. (2023). Quantifying source effects based on rainwater \u00e5180 from 10-year monitoring records in Southwest China. Applied Geochemistry, 155, 105706. https://doi.org/10.1016/j.apgeochem.2023.105706
- Yoshimura, K., Kanamitsu, M., Noone, D., & Oki, T. (2008). Historical isotope simulation using reanalysis atmospheric data. *Journal of Geophysical Research*, 113(D19), D19103. https://doi.org/10.1029/2008JD010074
- Yuan, D., Cheng, H., Edwards, R. L., Dykoski, C. A., Kelly, M. J., Zhang, M., et al. (2004). Timing, duration, and transitions of the last interglacial Asian monsoon. *Science*, 304(5670), 575–578. https://doi.org/10.1126/science.1091220
- Zhang, H., Zhang, X., Cai, Y., Sinha, A., Spötl, C., Baker, J., et al. (2021). A data-model comparison pinpoints Holocene spatiotemporal pattern of East Asian summer monsoon. *Quaternary Science Reviews*, 261, 106911. https://doi.org/10.1016/j.quascirev.2021.106911
- Zhang, H.-L., Yu, K.-F., Zhao, J.-X., Feng, Y.-X., Lin, Y.-S., Zhou, W., & Liu, G.-H. (2013). East Asian Summer Monsoon variations in the past 12.5 ka: High-resolution δ¹⁸O record from a precisely dated aragonite stalagmite in central China. *Journal of Asian Earth Sciences*, 73, 162–175. https://doi.org/10.1016/j.jseaes.2013.04.015

WANG ET AL. 12 of 13

- Zhang, W., Yan, H., Dodson, J., Cheng, P., Liu, C., Li, J., et al. (2018). The 9.2 ka event in Asian summer monsoon area: The strongest millennial scale collapse of the monsoon during the Holocene. Climate Dynamics, 50(7), 2767–2782, https://doi.org/10.1007/s00382-017-3770-2
- Zhao, J., Cheng, H., Cao, J., Sinha, A., Dong, X., Pan, L., et al. (2023). Orchestrated decline of Asian summer monsoon and Atlantic meridional overturning circulation in global warming period. The Innovation Geoscience, 1(1), 100011-9. https://doi.org/10.59717/j.xinn-geo.2023.
- Zheng, Z., Kuang, K., Wan, Q., & Cheddadi, R. (2020). How the Asian subtropical area became evergreen since the last Glacial Maximum. Past Global Changes Magazine, 28(1), 6-7. https://doi.org/10.22498/pages.28.1.6
- Zhong, W., Cao, J., Xue, J., & Ouyang, J. (2015). A 15,400-year record of climate variation from a subalpine lacustrine sedimentary sequence in the western Nanling Mountains in South China, Ouaternary Research, 84(2), 246-254. https://doi.org/10.1016/j.ygres.2015.06.002
- Zhu, C., Ma, C., Yu, S.-Y., Tang, L., Zhang, W., & Lu, X. (2010). A detailed pollen record of vegetation and climate changes in Central China during the past 16 000 years. Boreas, 39(1), 69-76. https://doi.org/10.1111/j.1502-3885.2009.00098.x

References From the Supporting Information

- Baertschi, P. (1976). Absolute 18O content of standard mean ocean water. Earth and Planetary Science Letters, 31(3), 341–344. https://doi.org/10. 1016/0012-821X(76)90115-1
- Brovkin, V., Raddatz, T., Reick, C., Claussen, M., & Gayler, V. (2009). Global biogeophysical interactions between forest and climate. Geophysical Research Letters, 36(7), L07405, https://doi.org/10.1029/2009GL037543
- Cheng, H., Edwards, R. L., Hoff, J., Gallup, C. D., Richards, D. A., & Asmerom, Y. (2000). The half-lives of uranium-234 and thorium-230. Chemical Geology, 169(1), 17-33. https://doi.org/10.1016/s0009-2541(99)00157-6
- Cheng, H., Edwards, R. L., Shen, C., Polyak, V. J., Asmerom, Y., Woodhead, J., et al. (2013). Improvements in ²³⁰Th dating, ²³⁰Th and ²³⁴U halflife values, and U-Th isotopic measurements by multi-collector inductively coupled plasma mass spectrometry. Earth and Planetary Science Letters, 371, 82-91. https://doi.org/10.1016/j.epsl.2013.04.006
- Chiang, J. C. H., Herman, M. J., Yoshimura, K., & Fung, I. Y. (2020). Enriched East Asian oxygen isotope of precipitation indicates reduced summer seasonality in regional climate and westerlies. Proceedings of the National Academy of Sciences, 117(26), 14745-14750. https://doi. org/10.1073/pnas.1922602117
- De Wit, J. C., Van der Straaten, C. M., & Mook, W. G. (1980). Determination of the absolute hydrogen isotopic ratio of V-SMOW and SLAP.
- $\label{eq:Geostandards Newsletter, 4(1), 33-36. https://doi.org/10.1111/j.1751-908X.1980.tb00270.x} Edwards, R. L., Chen, J., & Wasserburg, G. (1987). $^{238}U-^{234}U-^{230Th}-^{232}Th$ systematics and the precise measurement of time over the past 500,000 and the past 500,0$ years. Earth and Planetary Science Letters, 81(2-3), 175-192. https://doi.org/10.1016/0012-821x(87)90154-3
- Hendy, C. H. (1971). The isotopic geochemistry of speleothems—I. The calculation of the effects of different modes of formation on the isotopic composition of speleothems and their applicability as palaeoclimatic indicators. Geochimica et Cosmochimica Acta, 35(8), 801-824. https:// doi.org/10.1016/0016-7037(71)90127-X
- Hibler, W. D., III. (1979). A dynamic thermodynamic sea ice model. Journal of Physical Oceanography, 9(4), 815-846. https://doi.org/10.1175/ 1520-0485(1979)009<0815:ADTSIM>2.0.CO:2
- Jaffey, A. H., Flynn, K. F., Glendenin, L. E., Bentley, W. C., & Essling, A. M. (1971). Precision measurement of half-lives and specific activities 35U and ²³⁸U. Physical Review C, 4(5), 1889–1906. https://doi.org/10.1103/PhysRevC.4.1889
- Kanamitsu, M., Ebisuzaki, W., Woollen, J., Yang, S.-K., Hnilo, J., Fiorino, M., & Potter, G. L. (2002). NCEP-DOE AMIP-II reanalysis (R-2). Bulletin of the American Meteorological Society, 83(11), 1631-1644. https://doi.org/10.1175/BAMS-83-11-1631
- Kathayat, G., Sinha, A., Tanoue, M., Yoshimura, K., Li, H., Zhang, H., & Cheng, H. (2021). Interannual oxygen isotope variability in Indian summer monsoon precipitation reflects changes in moisture sources. Communications Earth & Environment, 2(1), 96. https://doi.org/10.1038/ s43247-021-00165-z
- Marsland, S. J., Haak, H., Jungclaus, J. H., Latif, M., & Röske, F. (2003). The max-Planck-institute global ocean/sea ice model with orthogonal curvilinear coordinates. Ocean Modelling, 5(2), 91-127. https://doi.org/10.1016/S1463-5003(02)00015-X
- Werner, M., Haese, B., Xu, X., Zhang, X., Butzin, M., & Lohmann, G. (2015). Glacial-interglacial changes of H₂¹⁸O, HDO and deuterium excessresults from the fully coupled Earth System Model ECHAM5/MPI-OM. Geoscientific Model Development Discussions, 8(10), 8835-8894. https://doi.org/10.5194/gmd-9-647-2016
- Xu, X., Werner, M., Butzin, M., & Lohmann, G. (2012). Water isotope variations in the global ocean model MPI-OM. Geoscientific Model Development, 5(3), 809-818, https://doi.org/10.5194/gmd-5-809-2012
- Yang, H., Johnson, K. R., Griffiths, M. L., & Yoshimura, K. (2016). Interannual controls on oxygen isotope variability in Asian monsoon precipitation and implications for paleoclimate reconstructions. Journal of Geophysical Research: Atmospheres, 121(14), 8410-8428. https:// doi.org/10.1002/2015JD024683

WANG ET AL. 13 of 13